Geologica Acta, Vol.4, Nº 4, 2006, 451-459
Available online at www.geologica-acta.com

geologica acta

A precise late Permian $^{40}Ar/^{39}Ar$ age for Central Iberian camptonitic lamprophyres

J.H. SCARROW [1] F. BEA [1] P. MONTERO [1] J.F. MOLINA [1] and A.P.M. VAUGHAN [2]

[1] Dept. Mineralogy and Petrology
University of Granada, Campus Fuentenueva, 18002 Granada, Spain. Scarrow E-mail: jscarrow@ugr.es

[2] British Antarctic Survey
High Cross, Madingley Road, Cambridge, CB3 0ET, U.K.

ABSTRACT

The Avila batholith of central Spain is composed, predominantly, of crustal-melt peraluminous granites cut by small-scale mafic alkaline bodies. Dating of the Gredos sector mafic camptonitic lamprophyre dykes was undertaken to constrain the Late Variscan tectonomagmatic evolution of the region. A well constrained late Permian, Capitanian, age of 264.5 ± 0.9 Ma was obtained by $^{40}Ar/^{39}Ar$ geochronology using amphibole separates. This new age clearly distinguishes the dykes from other episodes of alkaline mafic magmatism in the region. We suggest that the lamprophyre dykes were emplaced into already solidified granitoids after the tectonic control on magma generation changed from purely extensional to transtensional.

KEYWORDS | $^{40}Ar/^{39}Ar$ dating. Lamprophyres. Variscan. Central Iberia. Transtension.

INTRODUCTION

Interpretation of the Late Variscan geodynamic evolution of the Sierra de Gredos sector of the Avila batholith has been hampered by uncertainty regarding the age of camptonitic lamprophyre dykes cutting widespread crustal-melt granitoids of the region.

The dykes were originally suggested to be early Permian, Cisuralian, 283 ± 30 Ma by Rb/Sr (WR) (Bea et al., 1999; geologic time scale of Gradstein et al., 2004). Studies of comparable dykes suites cutting the more easterly Sierra de Guadarrama sector of the Avila batholith dated lamprophyres dykes at 277 ± 5 Ma by K/Ar (phlogopite) (Villaseca et al., 2004). Furthermore, notably in agreement with the current work, Perini et al. (2004) mentioned an unpublished date of 264 ± 1.3 Ma by $^{40}Ar/^{39}Ar$ (amphibole) for the Guadarrama sector lamprophyres. More recently, however, Orejana et al. (2005), whilst remarking on the poorly constrained nature of the geochronological data in the complex Guadarrama dyke swarm, approximately averaged the aforementioned dates and settled on an age of 270 Ma.

In this study we present a well-constrained late Permian, Capitanian, age of 264.5 ± 0.9 Ma determined by $^{40}Ar/^{39}Ar$ geochronology performed on amphibole mineral separates from Gredos sector mafic camptonitic lamprophyre dykes. This new date provides a fixed point in

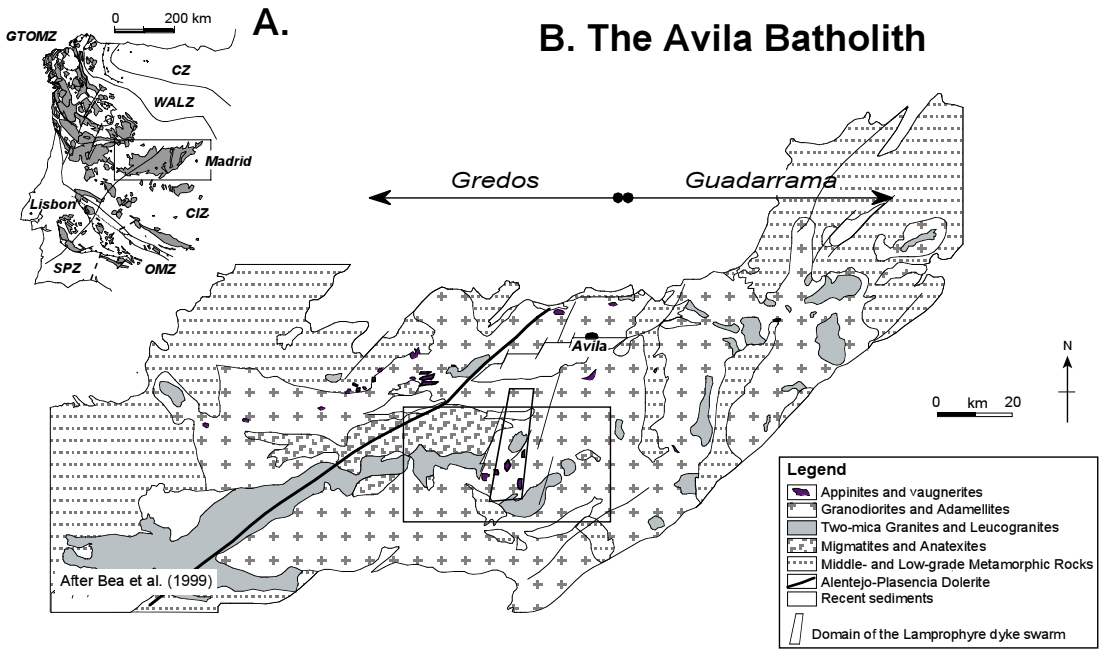

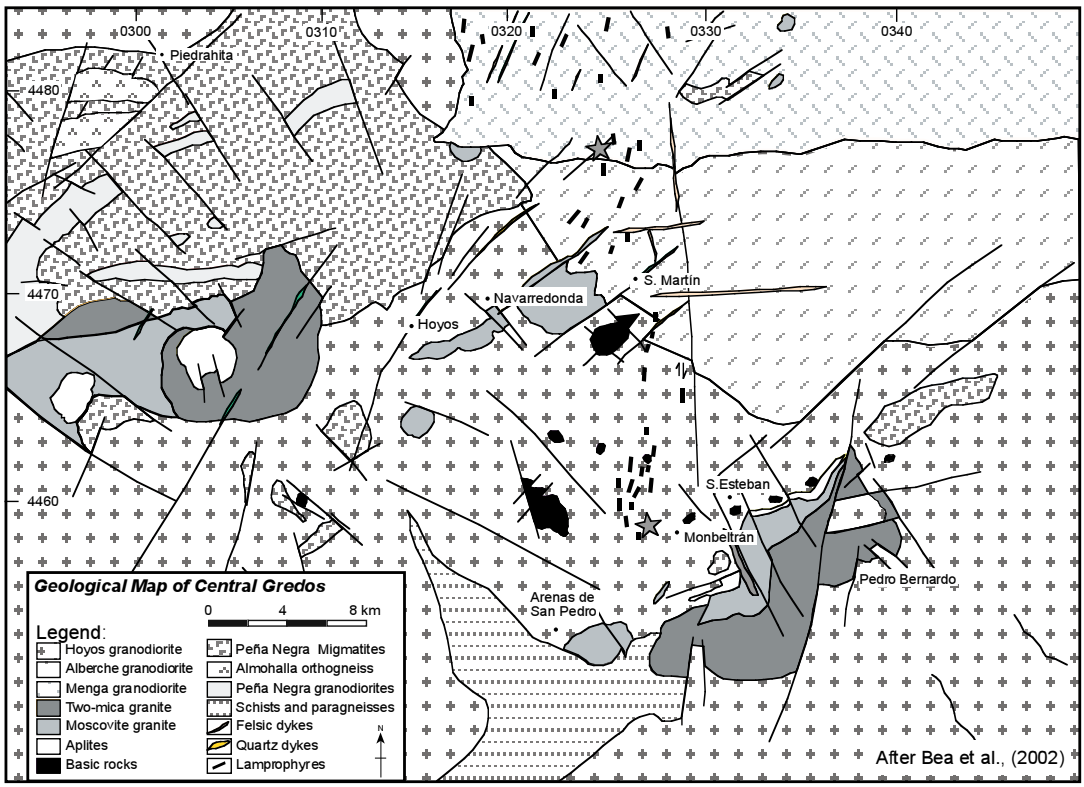

FIGURE 1 | **A) Scheme of the Iberian Massif. Grey areas represent plutonic, mostly granite-granodiorite, rocks. The main palaeogeographic zones (after Farias et al., 1987): CZ: Cantabrian Zone; WALZ: Western-Astur Leonian Zone; GTOMZ: Galicia Tras-os-Montes Zone; CIZ: Central Iberian Zone; OMZ: Ossa Morena Zone; SPZ: South Portuguese Zone. B) Geological map of the Avila batholith, the rectangle indicates the detail shown in C. C) Geological map of the Gredos Sector. Geochronological sampling localities are indicated by a grey star.**

the generation and, thus, tectonomagmatic evolution of the Iberian K-rich mafic rocks during the late Variscan.

GEOLOGICAL SETTING AND FIELD RELATIONS

The Central Iberian Zone, the central part of the Variscan chain in the Iberian Peninsula, comprises Proterozoic and early Palaeozoic metasediments and orthogneisses intruded by late Palaeozoic, ~330 to 300 Ma, collision-related granitoids (Martínez Catalán et al., 2004 and references mentioned therein) (Fig. 1). Early Variscan deformation in the region, ~360 to 350 Ma, almost doubled the thickness of the crust principally by underthrusting of the Ossa Morena Zone lower crust beneath Central Iberia (Azor et al., 1994). This main compressional stage was followed by an extensional phase and development of sub-horizontal shear zones associated with which was the main episode of granite production (Bea et al., 2003 and references mentioned therein).

The axis of the Central Iberian Zone in central Spain is dominated by the Avila batholith which crops out over ~13,000 km^2 (Bea et al., 2004; Fig. 1). The batholith is divided into two sectors: Gredos to the west and Guadarrama to the east. The Gredos sector, the focus of the current study, comprises numerous juxtaposed plutons of peraluminous granitoids which were divided into facies by Bea et al. (1999). In the core of the batholith, large low-pressure anatectic complexes crop out (Fig. 1). These granites and migmatites are cut by camptonitic alkaline lamprophyre dykes, forming broadly north-south trending swarms in eastern Guadarrama (Ubanell et al., 1984; Villaseca et al., 2002) and central Gredos (Bea and Corretgé, 1986; Bea et al., 1999) (Fig. 1).

The dykes of the Gredos sector, although typically laterally discontinuous and only 5 cm to 2 m thick, form a broad ~10 km wide, N-S to NNE-SSW trending swarm of some 100 steeply-dipping bodies (Bea et al., 1999; Fig. 1). To the north, in the Menga and Alberche granitoid facies the dykes form a broad swathe whereas the southerly extension of the swarm, in the Hoyos granitoid facies, is much more laterally restricted, ~3 km wide (Fig. 1).

Detailed mapping of the dykes reveals sharp contacts between the camptonites and host granitoids (Fig. 2A), the latter often having a diffuse band of episienite near the contact. However, despite the presence of such clear marker horizons, discontinuous and poor exposure of dyke contacts with the country rock make it difficult to determine the nature of the stress field during individual dyke emplacement. Nevertheless, on a regional scale, the difference between a N-S to NNW-SSE regional swarm

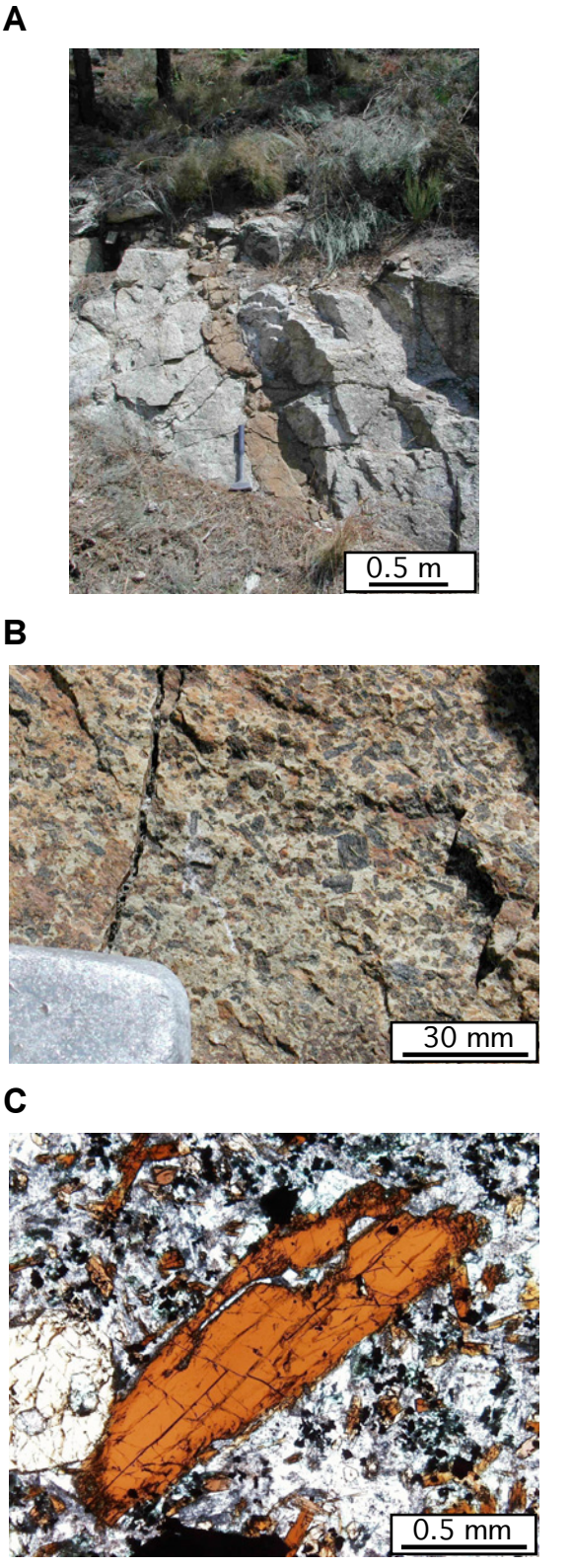

FIGURE 2 | **A) Outcrop photograph of a lamprophyre dyke cutting the Hoyos granodiorite. B) Hand specimen photograph of a typical camptonitic lamprophyre. Note the large, abundant, kaersutite amphibole phenocrysts. C) Thin section photomicrograph of dated lamprophyre, GREB-750. Note the lack of any indication of resorption, or reaction with the groundmass, of the kaersutite amphibole phenocryst. See text for details.**

trend and NNW-SSE to NW-SE local dyke trends indicates that the area was under bulk sinistral transtension during dyke emplacement. Rather than simple shear, the zone was also affected by a component of extension at a high angle to the strike-slip deformation (c.f., Dewey et al., 1998).

PETROGRAPHY AND MINERAL CHEMISTRY

Detailed descriptions of the petrography of the Gredos dykes have been published by Bea and coworkers (Bea and Corretgé, 1986; Bea et al., 1999). These authors noted the distinctive highly porphyritic nature, ~30 modal %, of the camptonites. The abundant phenocrysts include, large, up to a few cm length, kaersutite amphibole (Figs. 2B and 2C), zoned clinopyroxene with cores of Ti-Al-poor augite and Ti-Al-rich augite overgrowths, carbonate and Ti-magnetite and ulvöspinel. More evolved dykes may also contain plagioclase phenocrysts. Less common is Ti-phlogopite, evidence of textural disequilibrium with the mesostasis, including anhedreal embayed outlines and rims of coronitic kaersutite, led Bea and Corretgé (1986) to interpret the phlogopite as xenocrystic. The mesostasis is fine-grained panidiomorphic and composed of kaersutite, Ti-augite, plagioclase (An_{50-10}), alkali feldspar, Ti-magnetite, ilmenite, and pyrite, with sparse chalcopyrite and sphalerite, epidote, titanite and calcite. Such an assemblage is indicative of crystallization from an alkaline, Ti-rich, magma.

SAMPLES AND METHODS

Two representative camptonite dykes were selected for dating: one from the north of the swarm where it cuts the Menga granodiorite, the other from the south of the swarm where it cuts the Hoyos granodiorite (Fig. 1).

Amphibole phenocrysts could be obtained with relative ease from the porphyritic camptonitic lamprophyres (Fig. 2B). First, samples were cut into 1 cm thick slices and amphibole-rich zones snapped out with pliers. After rinsing in alcohol, ~70-80 mg of 0.25-0.5 mm fraction grains were hand-picked under a binocular microscope. These grains were then washed for 15 min in distilled water in an ultrasonic bath. One amphibole concentrate, Amp-1, was prepared from the northerly dyke (GRECH-2), and two amphibole concentrates, Amp-2 and Amp-3, were prepared from the southerly dyke (GREB-750).

Samples and monitor standard DRA1 (25.26 ± 0.07 Ma sanidine, Wijbrans et al. 1995) were irradiated for 55 hrs at the Beijing 49-2 reactor. To obtain the best control on irradiation of our samples, that is the best *J*-values for our $^{40}Ar/^{39}Ar$ geochronological studies, monitor DRA1 was packed in quartz tubes between every five unknown samples. The *J*-value uncertainty of 0.15% was propagated into the age calculations for every sample (Wijbrans et al., 1995; Qiu and Wijbrans, 2006). Prior to analysis, the system blank was reduced by heating the whole apparatus to 150ºC, for ~24 hours, using an infrared lamp and heating tape. The samples were step heated with a CO_2 laser (MIR10-50W) operated by New Wave Research© Laser Ablation System version 1.8.13.0 software. Correction factors for interfering argon isotopes derived from Ca and K are: $(^{39}Ar/^{37}Ar)_{Ca} = 8.984 \times 10^{-4}$, $(^{36}Ar/^{37}Ar)_{Ca} = 2.673 \times 10^{-4}$ and $(^{40}Ar/^{39}Ar)_K = 5.97 \times 10^{-3}$. Two SorbAC NP10 pumps purified the released gases. One operated at ~400ºC and the other at room temperature. The purification time was 5 min for amphibole. The purified gas was analyzed for argon isotopes in a VG5400-Ar mass spectrometer operated using Noble Gas Software (version 2.93). The $^{40}Ar/^{39}Ar$ data were reduced, and graphs were produced, using the ArArCALC software package (http://earthref.org/tools/ararcalc/index.html) which consists of Visual Basic® routines that operate as add-ins in Microsoft Excel®.

RESULTS

Fresh, inclusion-free, kaersutite phenocrysts are euhedral and apparently in textural and compositional equilibrium with their host groundmass in which, notably, the amphibole is also kaersutitic (Fig. 2C). In the absence of petrographic or geochemical evidence for secondary post-solidification processes, that could potentially cause geochronological resetting, dates obtained from the kaersutite phenocrysts should constrain the age of crystallization of the K-rich mafic camptonite dykes. This supposition was investigated using $^{40}Ar/^{39}Ar$ dating.

Three kaersutite phenocryst concentrates from two camptonite dykes yielded well-defined plateau ages which overlap within error, ranging from 264.3 ± 0.9 Ma to 264.6 ± 1.6 (Fig. 3, Tables 1 and 2). Although there is no uniform convention on the definition of a plateau in $^{40}Ar/^{39}Ar$ dating (McDougall and Harrison, 1999) we took the definition of Dallmeyer and Lecorche (1990) who considered that a plateau may be established when "ages defined by two or more contiguous gas fractions (with similar K/Ca ratios) each representing >4% of the total ^{39}Ar evolved (and together consisting of >50% of the total quantity of ^{39}Ar evolved) are mutually similar within a ± 1% intralaboratory uncertainty". Our plateaux meet these criteria, the $^{40}Ar/^{39}Ar$ age spectra produced by stepped heating with a CO_2 laser are flat, concordant, uniform release patterns with 85-100% of gas yielding the plateaux (Fig. 3A, Tables 1 and 2). Such flat age spectra

indicate uniform ^{40}Ar distribution inside the crystal lattice of the amphiboles implying that the samples were closed systems since their crystallization, that is undisturbed by physical or chemical processes since cooling through their Ar closure temperature, ~ 500ºC for calcic amphibole (MacDougall and Harrison, 1999). Accordingly, the amphiboles had relatively constant K/Ca over 98-100% of $^{39}Ar_K$ released for the three samples (Fig. 3B). In addition, the absence of "saddle-shaped" spectra rules out a significant component of excess ^{40}Ar, i.e., not formed by in-situ decay of ^{40}K. Furthermore, the total fusion and isochron ages for the three mineral separates are in excellent agreement, overlapping within error, with the plateau ages (Fig. 3, Table 2). Therefore, we conclude that the well-constrained late Permian, Capitanian, age of 264.5 ± 0.9 Ma reflects the time of cooling and, assuming that this was rapid, crystallization of the Gredos sector mafic camptonitic lamprophyre dykes.

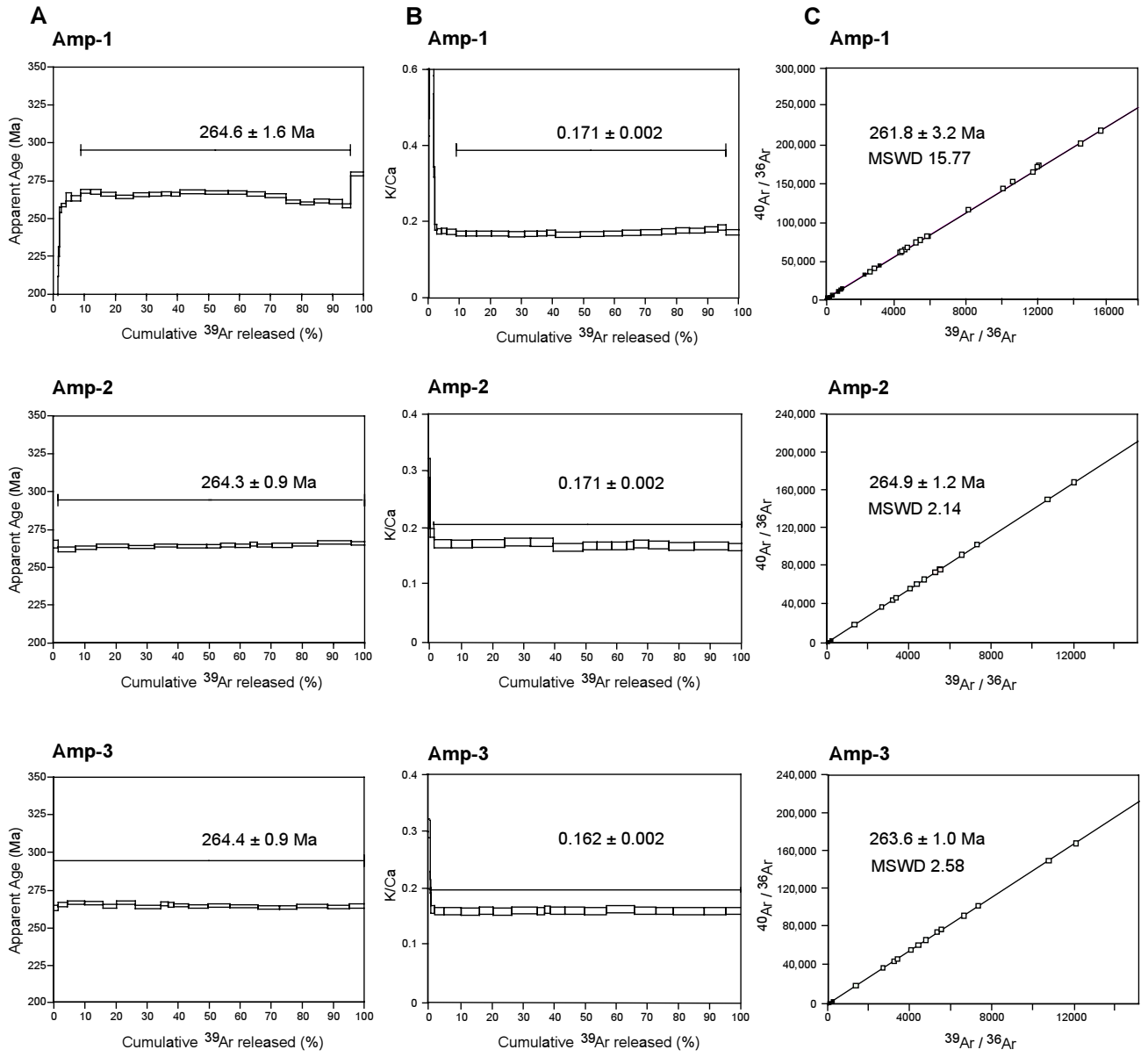

FIGURE 3 | **Age spectra for kaersutite phenocrysts from two representative Central Iberian camptonite dykes, one from the north of the regional swarm (GRECH-2: Amp-1) the other from the south (GREB-750: Amp-2 and Amp-3). B) Calculated K/Ca for Amp-1, Amp-2 and Amp-3. The plateaux are defined by over 98-100% of $^{39}Ar_K$ released for the three samples. The coefficient that transfers the ratio of production rate of $^{39}Ar_K/^{37}Ar$ into K/Ca ratio is 0.43. C) Isochron plots for Amp-1, Amp-2 and Amp-3. Note the agreement, within error, with plateau ages. Open symbols, defining the line, were used to calculate the isochron, solid symbols were not used in the calculation. See text for details.**

TABLE 1 | **$^{40}Ar/^{39}Ar$ dating results.**

Step	Laser power (W)	$^{36}Ar_{air}$	$^{37}Ar_{Ca}$	$^{38}Ar_{Cl}$	$^{39}Ar_{K}$	$^{40}Ar^{*}$	Age (Ma ± 2σ)	$^{40}Ar^{*}$ (%)	$^{39}Ar_{K}$ (%)	K/Ca	± 2σ
Kaersutite Amp-1											
1	0.69	0.000009	0.000478	0.000001	0.000498	0.00505	196.1 ± 7.5	66.81	0.19	0.448	± 0.023
2	1.14	0.000012	0.000719	0.000002	0.001083	0.00935	168.0 ± 2.8	72.92	0.42	0.648	± 0.026
3	1.37	0.000005	0.000357	0.000000	0.000730	0.00611	163.1 ± 3.3	79.10	0.28	0.879	± 0.037
4	1.59	0.000005	0.000326	0.000001	0.000756	0.00689	176.8 ± 2.2	83.64	0.29	0.996	± 0.040
5	1.82	0.000003	0.000370	0.000000	0.000663	0.00663	192.9 ± 2.2	88.39	0.26	0.771	± 0.032
6	2.04	0.000003	0.000429	0.000001	0.000557	0.00625	215.5 ± 3.5	88.15	0.22	0.558	± 0.023
7	2.26	0.000002	0.000830	0.000001	0.000636	0.00759	228.1 ± 3.2	93.63	0.25	0.33	± 0.013
8	2.48	0.000003	0.004337	0.000003	0.001865	0.02512	255.6 ± 1.8	96.88	0.72	0.185	± 0.007
9	2.61	0.000005	0.009928	0.000007	0.004031	0.05503	258.8 ± 1.2	97.47	1.56	0.175	± 0.007
10	2.74	0.000001	0.010036	0.000008	0.004104	0.05733	264.4 ± 2.8	99.28	1.59	0.176	± 0.007
11	2.91	0.000003	0.019077	0.000013	0.007674	0.10674	263.3 ± 1.6	99.01	2.97	0.173	± 0.007
12*	3.04	0.000002	0.021812	0.000018	0.008548	0.12111	267.9 ± 1.4	99.48	3.3	0.169	± 0.007
13*	3.17	0.000003	0.021991	0.000018	0.008614	0.12193	267.7 ± 1.5	99.21	3.33	0.168	± 0.007
14*	3.34	0.000002	0.031314	0.000025	0.012282	0.17265	266.0 ± 1.2	99.57	4.75	0.169	± 0.007
15*	3.46	0.000003	0.036596	0.000030	0.014370	0.20060	264.3 ± 1.1	99.59	5.56	0.169	± 0.007
16*	3.59	0.000003	0.034075	0.000028	0.013215	0.18560	265.8 ± 1.3	99.50	5.11	0.167	± 0.007
17*	3.76	0.000001	0.026946	0.000023	0.010526	0.14796	266.0 ± 1.3	99.70	4.07	0.168	± 0.007
18*	3.88	0.000002	0.020459	0.000017	0.008032	0.11308	266.4 ± 1.2	99.50	3.1	0.169	± 0.007
19*	4.17	0.000001	0.018117	0.000013	0.007184	0.10102	266.1 ± 1.4	99.60	2.78	0.171	± 0.007
20*	4.38	0.000004	0.054227	0.000041	0.020837	0.29482	267.6 ± 1.3	99.50	8.06	0.165	± 0.006
21*	4.58	0.000002	0.050306	0.000042	0.019620	0.27717	267.2 ± 1.1	99.80	7.58	0.168	± 0.007
22*	4.79	0.000001	0.039953	0.000033	0.015656	0.22124	267.3 ± 1.2	99.80	6.05	0.168	± 0.007
23*	4.99	0.000001	0.038415	0.000032	0.015235	0.21447	266.3 ± 1.4	99.79	5.89	0.171	± 0.007
24*	5.19	0.000002	0.042968	0.000036	0.017140	0.24008	265.1 ± 1.2	99.75	6.63	0.172	± 0.007
25*	5.39	0.000001	0.030140	0.000025	0.012223	0.16839	261.0 ± 1.1	99.82	4.73	0.174	± 0.007
26*	5.58	0.000001	0.027593	0.000023	0.011321	0.15534	260.0 ± 1.0	99.81	4.38	0.176	± 0.007
27*	5.78	0.000002	0.031305	0.000025	0.012828	0.17712	261.6 ± 1.3	99.59	4.96	0.176	± 0.007
28*	6.17	0.000001	0.026167	0.000022	0.010892	0.15016	261.2 ± 1.4	99.78	4.21	0.179	± 0.007
29*	8.02	0.000003	0.015710	0.000012	0.006740	0.09181	258.3 ± 1.3	99.11	2.61	0.184	± 0.007
30*	18.29	0.000012	0.027065	0.000020	0.010815	0.16042	279.6 ± 1.3	97.83	4.18	0.172	± 0.007
Kaersutite Amp-2											
1	3.10	0.000040	0.001810	0.000000	0.001290	0.02682	379.2 ± 13.2	67.93	0.45	0.305	± 0.017
2	4.35	0.000020	0.007930	0.000010	0.003540	0.04995	265.2 ± 2.6	90.10	1.23	0.192	± 0.008
3*	4.97	0.000010	0.039980	0.000030	0.016070	0.22367	261.8 ± 1.7	98.40	5.59	0.173	± 0.007
4*	5.59	0.000010	0.047610	0.000030	0.019100	0.26699	262.8 ± 1.1	99.30	6.64	0.172	± 0.007
5*	5.90	0.000010	0.073600	0.000050	0.029650	0.41665	264.1 ± 1.1	99.44	10.31	0.173	± 0.007
6*	6.21	0.000000	0.058570	0.000040	0.023970	0.33588	263.4 ± 1.1	99.56	8.34	0.176	± 0.007
7*	6.52	0.000000	0.051020	0.000040	0.020820	0.29274	264.3 ± 1.1	99.51	7.24	0.175	± 0.007
8*	7.14	0.000010	0.070740	0.000050	0.027420	0.38486	263.7 ± 1.0	99.17	9.54	0.167	± 0.007
9*	7.45	0.000000	0.032720	0.000020	0.012840	0.18026	263.8 ± 1.1	99.33	4.47	0.169	± 0.007
10*	7.76	0.000000	0.034040	0.000030	0.013400	0.18879	264.7 ± 1.3	99.48	4.66	0.169	± 0.007
11*	8.07	0.000000	0.034330	0.000020	0.013480	0.18945	264.1 ± 1.1	99.43	4.69	0.169	± 0.007
12*	8.38	0.000000	0.017420	0.000010	0.006900	0.09742	265.1 ± 1.2	99.58	2.40	0.170	± 0.007
13*	8.69	0.000000	0.033890	0.000020	0.013610	0.19150	264.3 ± 1.1	99.78	4.74	0.173	± 0.007
14*	9.93	0.000000	0.046350	0.000030	0.018390	0.25896	264.5 ± 1.4	99.76	6.40	0.171	± 0.007
15*	11.80	0.000000	0.059830	0.000050	0.023380	0.32979	265.0 ± 1.1	99.64	8.13	0.168	± 0.007
16*	15.52	0.000010	0.078810	0.000060	0.031030	0.43997	266.3 ± 1.1	99.58	10.79	0.169	± 0.007
17*	18.62	0.000000	0.032390	0.000030	0.012570	0.17770	265.6 ± 1.1	99.67	4.37	0.167	± 0.007

TABLE 1 | **Continued.**

Step	Laser power (W)	$^{36}Ar_{air}$	$^{37}Ar_{Ca}$	$^{38}Ar_{Cl}$	$^{39}Ar_{K}$	$^{40}Ar^{*}$	Age (Ma ± 2σ)	$^{40}Ar^{*}$ (%)	$^{39}Ar_{K}$ (%)	K/Ca	± 2σ
Kaersutite Amp-3											
1	2.48	0.000020	0.000170	0.000000	0.000110	0.00243	411.7 ± 63.3	26.99	0.04	0.277	± 0.046
2	3.72	0.000030	0.001040	0.000000	0.000500	0.00755	283.6 ± 14.1	46.98	0.18	0.205	± 0.012
3*	4.35	0.000000	0.009540	0.000010	0.003630	0.05076	262.9 ± 1.7	99.48	1.29	0.164	± 0.007
4*	4.97	0.000010	0.022280	0.000020	0.008340	0.11753	265.2 ± 1.4	98.23	2.96	0.161	± 0.006
5*	5.59	0.000000	0.041720	0.000030	0.015610	0.22101	266.3 ± 1.1	99.62	5.55	0.161	± 0.006
6*	5.90	0.000000	0.045020	0.000040	0.016730	0.23674	266.1 ± 1.2	99.69	5.95	0.160	± 0.006
7*	6.21	0.000000	0.031970	0.000030	0.012010	0.16852	264.0 ± 1.2	99.65	4.27	0.162	± 0.006
8*	6.52	0.000000	0.045900	0.000040	0.017050	0.24153	266.4 ± 1.2	99.71	6.06	0.160	± 0.006
9*	6.83	0.000000	0.061790	0.000050	0.023290	0.32591	263.4 ± 1.1	99.74	8.28	0.162	± 0.006
10*	7.14	0.000000	0.017420	0.000020	0.006510	0.09188	265.6 ± 1.4	99.43	2.31	0.161	± 0.006
11*	7.45	0.000000	0.014470	0.000010	0.005500	0.07750	265.0 ± 1.6	99.68	1.96	0.164	± 0.007
12*	7.76	0.000000	0.034510	0.000030	0.013000	0.18284	264.7 ± 1.1	99.68	4.62	0.162	± 0.006
13*	8.07	0.000000	0.047640	0.000040	0.017950	0.25166	263.9 ± 1.1	99.81	6.38	0.162	± 0.006
14*	8.38	0.000000	0.052200	0.000040	0.019540	0.27465	264.5 ± 1.1	99.84	6.95	0.161	± 0.006
15*	9.00	0.000000	0.066230	0.000050	0.025330	0.35536	264.0 ± 1.0	99.80	9.01	0.164	± 0.006
16*	9.31	0.000000	0.051740	0.000040	0.019420	0.27150	263.2 ± 1.1	99.80	6.90	0.161	± 0.006
17*	9.93	0.000000	0.042200	0.000030	0.015830	0.22149	263.3 ± 1.1	99.70	5.63	0.161	± 0.006
18*	11.17	0.000000	0.074460	0.000060	0.027910	0.39202	264.3 ± 1.1	99.75	9.92	0.161	± 0.006
19*	12.42	0.000000	0.052450	0.000040	0.019660	0.27527	263.6 ± 1.1	99.79	6.99	0.161	± 0.006
20*	14.89	0.000000	0.035640	0.000030	0.013370	0.18769	264.3 ± 1.4	99.55	4.75	0.161	± 0.006

* Steps included in the age calculations.
The argon isotopes are listed in volts.
Laser power is the power to sample.
$^{40}Ar^{*} = {}^{40}Ar_{m} - 295 * {}^{36}Ar_{m}$, where m indicates measured data.

TABLE 2 | **Kaersutite $^{40}Ar/^{39}Ar$ ages for Central Iberian camptonitic lamprophyres.**

Sample	Locality UTM Coordinates	Mineral	J	Weight (mg)	Grain size (mm)	Total Fusion age (Ma ± 2σ)	Isochron age (Ma ± 2σ)	MSWD Isochron age	Weighted Plateau age (Ma ± 2σ)	MSWD Plateau age	% ^{39}Ar used
GRECH-2 (Amp-1)	032420 447700	Krs	0.01130	3	0.25-0.50	264.0 ± 0.8	261.8 ± 3.2	15.77	264.6 ± 1.6	23.5	94
GREB-750 (Amp-2)	032750 445870	Krs	0.01122	3	0.25-0.50	264.8 ± 0.8	264.9 ± 1.2	2.14	264.3 ± 0.9	3.27	98
GREB-750 (Amp-3)	032750 445870	Krs	0.01123	3	0.25-0.50	264.5 ± 0.8	263.6 ± 1.0	2.58	264.4 ± 0.9	3.31	100

UTM Universal Transverse Mercator Coordinates.
Krs Kaersutite.
J is the irradiation parameter.

DISCUSSION

To consider the implications of the different expressions of Variscan magmatism and, in particular, the timing of the camptonite dyke emplacement, it is relevant to summarize the relative ages of the main magmatic episodes in the Gredos sector of the Avila batholith. Granitic melt production in the region took place during the Early Carboniferous to Early Permian, over 55 million years from 352 to 297 Ma (Montero et al., 2004a). A limited melting event occurred coincident with the main Variscan collision at ~350 Ma. Later extensive anatexis,

at ~330 Ma, produced melts which pooled in migmatite complexes and, at ~320 Ma, segregated into small scale leucogranite bodies. Subsequently, from 325 to 305 Ma, extensional collapse-related sub-horizontal shear zones provoked extensive in-situ lower- and, in particular, mid-crustal melting throughout the region. After peaking at 309 Ma melt production decreased significantly and had stopped completely by 297 Ma (Montero et al., 2004a). Superimposed upon this widespread granitic magmatism was a punctual episode of originally alkaline mafic magmatism, ~312 Ma, currently preserved in heavily contaminated localized stocks and enclaves of appinitic composition (Bea et al., 2004; Montero et al., 2004b). So, the new, late Permian, $^{40}Ar/^{39}Ar$ age of 264.5 ± 0.9 Ma, for the camptonite dykes clearly fixes their emplacement as younger than the main Variscan magmatism in the region.

The marked change in emplacement style of alkaline mafic melts from "mixed" stocks at 312 Ma to "pure" dykes at 264 Ma, implies a change in regional tectonic regime. During extensional collapse sub-horizontal shear zones facilitated crustal melting (Montero et al., 2004b) so small-scale melts of the metasomatized mantle lithosphere could only proceed to the surface with some difficulty. These melts would have interacted with the ponded, mid-crustal melt, granitic magma resulting in the formation of the aforementioned mixed appinitic stocks. By contrast, we suggest that the camptonite dykes emplaced at ~264 Ma in the already solidified granitoids soon after the tectonic control changed from purely extensional to transtensional. Within this context opening lithosphere-scale rheidal fractures would have facilitated the passage of metasomatized mantle lithosphere melts to shallow depths.

Vaughan and Scarrow (2003) proposed that K-rich mantle metasomatism controls the initiation and position of lithosphere-scale strike-slip shear zones. This idea is of particular interest in geodynamic reconstructions given the suggestion of Bonin et al. (1998) that K-rich magmatism is commonly related to strike-slip faulting in a post-orogenic setting. We propose, more specifically, that K-rich mafic magmatism is in fact typical in *tardi-orogenic settings* related to the main collisional process as a last-gasp release of melts of metasomatized lithopsheric mantle in a final melt-focussed transtensional judder once other larger-scale tectonomagmatic events, and thus potentially-masking magmatism, has been switched off.

The suggestion, from the current work, that tardi-orogenic lamprophyres act as a geodynamic marker of the end of extensional collapse and a change of tectonic regime to transtension merits investigation at a broader scale.

CONCLUSIONS

- A well constrained late Permian, Capitanian, age of 264.5 ± 0.9 Ma is assigned to the Gredos sector mafic camptonitic lamprophyre dykes.

- This age is interpreted as the time of cooling and, assuming that this was rapid, crystallization of the mafic dykes.

- The Central Iberian tardi-orogenic lamprophyres act as a geodynamic marker for a change from pure extensional to transtensional control of tapping of alkaline mafic magmas from the metasomatized mantle lithosphere.

ACKNOWLEDGEMENTS

The authors are grateful to H. N. Qiu of The Chinese Academy of Sciences, Guangzhou, China for undertaking the $^{40}Ar/^{39}Ar$ analysis. Professors C. Galindo Francisco, A. Iriondo and G. Ruffet are thanked for detailed reviews that helped us to considerably improve the manuscript. This work has been supported by the Spanish CICYT project CGL2005-05863.

REFERENCES

Azor, A., González Lodeiro, F., Simancas, F., 1994. Tectonic evolution of the boundary between the Central Iberian and Ossa-Morena zones (Variscan belt, southwest Spain). Tectonics, 13, 45-61.

Bea, F., Corretgé, L.G., 1986. Petrography, geochemistry, and differentiation models of lamprophyres from Sierra de Gredos, Central Spain. Hercynica, 2, 1-15.

Bea, F., Montero, P., Molina, J.F., 1999. Mafic precursors, peraluminous granitoids, and late lamprophyres in the Avila batholith: A model for the generation of Variscan batholiths in Iberia. Journal of Geology, 107, 399-419.

Bea, F., Montero, P., Scarrow, J.H., Molina, J.F., 2002. The Gredos Sector of the Avila batholith, Central Iberia: An introduction. Gredos Seminar on Crustal Granites. Navarredonda de Gredos, 7-12 September 2002.

Bea, F., Montero, P., Zinger, T., 2003. The Nature and Origin of the Granite Source Layer of Central Iberia: Evidence from Trace Element, Sr and Nd Isotopes, and Zircon Age Patterns. Journal of Geology, 111, 579-595.

Bea, F., Villaseca, C., Bellido, F., 2004. El batolito de Avila (Sistema Central Español). In: Vera, J.A. (ed.). Geología de España. Madrid, Sociedad Geológica e Instituto Geológico y Minero de España, 101-110.

Bonin, B.L., Azzouni-Sekkal, A., Bussy, F., Ferrag, S., 1998. Alkali-calcic and alkaline post-orogenic (PO) granite magmatism: petrologic constraints and geodynamic settings. Lithos, 45, 45-70.

Dallmeyer, R.D., Lecorche, J.P., 1990. $^{40}Ar/^{39}Ar$ polyorogenic mineral age record in the northern Mauritanide orogen, West Africa. Tectonophysics, 177, 81-107.

Dewey, J.F., Holdsworth, R.E., Strachan, R.A., 1998. Transpression and transtension zones. In: Holdsworth, R.E., Strachan, R.A., Dewey, J.F. (eds.). Continental Transpressional and Transtensional Tectonics. Geological Society, London, Special Publication, 135, 1-14.

Farias, P., Gallastegui, G., González Lodeiro, F., Marquínez, J., Martín-Parra, L.M., Martínez Catalán, J.R., de Pablo Maciá, J.G., Rodríguez Fernández, L.R., 1987. Aportaciones al conocimiento de la litoestratigrafía y estructura de Galicia Central. Museu e Laboratório Mineralúgico e Geológico, Faculdade de Ciéncias, Universidade do Porto, Memórias, 1, 411-431.

Gradstein, F.M., Ogg, J.G., Smith, A.G., Agterberg, F.P., Blleker, W., Cooper, R.A., Davydov, V., Gibbard, P., Hinnov, L.A., House, M.R., Lourens, L., Luterbacher, H.P., McArthur, J., Melchin, M.J., Robb, L.J., Shergold, J., Villeneuve, M., Wardlaw, B.R., Ali, J., Brinkhuis, H., Hinden, F.J., Hooker, J., Howarrh, R.J., Knoll, A.H., Laskar, J., Monechi, S., Plumb, K.A., Powell, J., Raffi, I., Röhl, U., Sadler, P., Sanfilipp, A., Schmitz, B., Shakleton, N.J., Shield, G.A., Van Dam, J., van Kolfschoten, T., Veizer, J., Wilson, D., 2005. A Geological Time Scale 2004, Cambridge, Cambridge University Press, 589 pp.

MacDougall, I., Harrison, M.T., 1999. Geochronology and Thermochronology by the $^{40}Ar/^{39}Ar$ method. Oxford University Press, 269 pp.

Martínez Catalán, J.R., Martínez Poyatos, D., Bea, F., 2004. La Zona Centroibérica, Introducción. In: Vera J.A. (ed.). Geología de España. Madrid, Sociedad Geológica e Instituto Geológico y Minero de España, 68-69.

Montero, P., Bea, F., Zinger, T.F., Scarrow, J.H., Molina, J.F., Whitehouse, M.J., 2004a. 55 Million Years of Continuous Anatexis in Central Iberia: Single Zircon Dating of the Peña Negra Complex. Journal of the Geological Society, London, 161, 255-264

Montero, P., Bea, F., Zinger, T.F., 2004b. Edad $^{207}Pb/^{206}Pb$ en cristal único de circón de las rocas máficas y ultramáficas del sector de Gredos, Batolito de Ávila (Iberia Central). Revista de la Sociedad Geologica de España, 17, 157-165.

Orejana, D., Villaseca, C., Paterson, B.A., 2005. Geochemistry of pyroxenitic and hornblenditic xenoliths in alkaline lamprophyres from the Spanish Central System. Lithos, 86, 167-196.

Perini, J., Cabria, M., López-Ruiz, J., Doblas, M., 2004. Carboniferous-Permian mafic magmatism in the Variscan belt of Spain and France: implications for mantle sources In: Wilson, M., Neumann, E.R., Davies, G.R., Timmerman, M.J., Heeremans M., Larsen, B.T. (eds.). Permo-Carboniferous Magmatism and Rifting in Europe, Geological Society of London, Special Publication, 223, 415-438.

Qiu H.N., Wijbrans J.R., 2006. Paleozoic ages and excess ^{40}Ar in garnets from the Bixiling eclogite in Dabieshan, China: new insights from $^{40}Ar/^{39}Ar$ dating by stepwise crushing. Geochimica et Cosmochimica Acta, 70, 2354-2370.

Vaughan, A.P.M., Scarrow, J.H., 2003. K-rich mantle metasomatism control of localization and initiation of lithospheric strike-slip faulting. Terra Nova, 15, 163-169.

Villaseca, C., Orejana, D., Pin, C., López García, J.A., Andonaegui, P., Encina, L., 2002. Estimación de la composición del manto subcontinental en el centro de España a partir de los materiales básicos hercínicos y post-hercínicos del Sistema Central Español. Geogaceta, 32, 15-18.

Villaseca, C., Huertas M.J., Orejana, D., Carracedo, M., Jiménez San Pedro J., Scarrow, J.H., 2004. Magmatismo filoniano tardi- y postvarisco. In: Vera J.A. (ed.). Geología de España. Madrid, Sociedad Geológica e Instituto Geológico y Minero de España, 124-128.

Wijbrans, J.R., Pringle, M.S., Koppers, A.A.P., Scheveers, R., 1995. Argon geochronology of small samples using the vulkaan argon laserprobe. Proceedings of the Koninklijke Nederlandse Akademie van Wetenschappen-Biological Chemical Geological Physical and Medical Sciences, 98, 185-218.

Manuscript received March 2006;
revision accepted August 2006.